Experimental study of low-frequency electrostatic fluctuations in a magnetized toroidal plasma

Frank J. Øynes,* Ole-Morten Olsen, Hans L. Pécseli,† Åshild Fredriksen, and Kristoffer Rypdal
Institute of Mathematical and Physical Sciences, University of Tromsø, N-9037 Tromsø, Norway
(Received 26 June 1997)

An experimental study of low-frequency electrostatic fluctuations is presented for a plasma produced by a steady-state discharge in a magnetized toroidal plasma device without a rotational transform. A significant intermittency of the fluctuations is observed. Thus the evolution and propagation of large coherent vortical structures is demonstrated by a conditional sampling technique. The flutelike nature of the structures is explicitly demonstrated. The analysis includes measurements of fluctuations in plasma density, electric potential, and electron temperature. The relevance of the observations to anomalous transport in the device is pointed out. The performance of the conditional sampling technique is compared to a simple correlation analysis by a Monte Carlo simulation. [S1063-651X(98)14402-1]

PACS number(s): 52.35.Ra, 52.25.Fi, 52.25.Gj

I. INTRODUCTION

In this paper we describe experimental studies of fluctuations observed in the toroidal Blaamann device at the University of Tromsø, Norway, emphasizing the role of large scale electrostatic vortices in determining the radial plasma transport across magnetic field lines.

A toroidally magnetized, collisionless plasma without a toroidal current and no rotational transform, such as the one in the Blaamann device, does not possess a nontrivial ideal magnetohydrodynamics (MHD) equilibrium [1]. A quasi-steady-state plasma distribution can nevertheless be produced by maintaining a discharge to balance losses of plasma and electric charge. A thorough description and discussion of this type of discharges was given in [2]. It was observed that the plasma state was strongly influenced by the charge injected via the filament cathode. Estimates show that classical transport (in our case dominated by ion-neutral collisions) is not sufficient to provide the cross-field current necessary to compensate the charge injected into the toroidal magnetic flux tube intersecting the filament. It was also shown that classical transport is insufficient to compensate the charge accumulation due to guiding center drifts of electron and ions (∇B and curvature drifts), although the latter accumulation is small compared to that arising from electron injection. Hence, for nontrivial, inhomogeneous plasma states the radial cross-field current is anomalous in nature. The sum of the radial pressure force and the centrifugal force on the plasma is balanced by the $\mathbf{j}_\theta \times \mathbf{B}$ force which arises from the sum of the poloidal diamagnetic current $\mathbf{j}_{\mathbf{d}\theta}$ and the current from the poloidal component of the ion polarization drift. Not quite so obvious is the existence of an anomalous viscous force arising from the fluctuation contribution to $\nabla \cdot \mathbf{T}$, where $\mathbf{T} = \overline{\rho_{\mathbf{m}} \mathbf{v}\mathbf{v}}$ is the Reynolds stress tensor arising from inclusion of ion inertia in the momentum equation [2]. Here ρ_m is the fluid mass density and $\mathbf{v}$ is the fluid velocity.

In this paper we shall use the notion of *stationary equilibrium*—meaning a plasma with a stationary flow ($\partial_t \mathbf{v} = 0$, $\partial_t \rho_m = 0$, etc.), and the notion of *fluctuating equilibrium*—meaning a fluctuating state with stationary mean values. It is important to realize that a finite plasma density at the boundary is a prerequisite for the existence of a stationary—as well as a fluctuating—MHD equilibrium. This can be seen from a simple generalization of the nonexistence proof of Tasso, Green, and Zeehrfeld [1], and is done by proving that the following four assumptions lead to a contradiction: (a) vanishing boundary density ρ_m and boundary plasma pressure p, (b) $p > 0$ in at least one point in the plasma, (c) stationary or fluctuating equilibrium, and (d) MHD equations satisfied.

First we note that such a contradiction follows immediately if there are sources for mass (S_m) or charge (S_ρ) in the plasma. Assumption (a) implies that the mass flux $\rho_m \mathbf{v}$ vanishes on the boundary, hence the mass source yields mass accumulation, contradicting the equilibrium assumption (c). With respect to charge we note that ∇p is perpendicular to the boundary, and since $\rho_m = 0$ makes the inertia term in the momentum equation vanish on the boundary, this equation reduces to $\mathbf{j} \times \mathbf{B} = \nabla p$, implying that the current density $\mathbf{j}$ is parallel to the boundary surface. This means that there is no current flowing out of the plasma, and the source will increase the total charge, again contradicting assumption (c).

Having established the nonexistence of stationary and fluctuating equilibria with vanishing boundary density if sources are present, we proceed assuming no sources. From the MHD momentum equation, Ampére's law, and the mass continuity equation, using assumption (a), Tasso, Green, and Zeehrfeld [1] arrived at the relation

$$\int [2p + \rho_m (v_\varphi^2 + v_R^2)] d^3r = \frac{\partial}{\partial t} \int \rho_m v_R R d^3r, \qquad (1)$$

where v_R is the velocity along the major radius, and v_φ is the velocity in the toroidal direction. In a stationary equilibrium the right hand side of this equation vanishes, while assumption (b) implies that the left hand side is positive. In a fluctuating equilibrium, the time average of the right hand side vanishes, while the time average on the left is positive. In

*Present address: Spacetec A/S, Prestevannsveien 38, N-9005 Tromsø, Norway.
†Also at Physics Institute, University of Oslo, Box 1048 Blindern, N-0316 Oslo, Norway.

both cases we have a contradiction, which concludes the proof of nonexistence of stationary or fluctuating equilibrium with vanishing density on the boundary.

These considerations show that the experimental fluctuating equilibria reported in this paper exist only if the plasma is in contact with the boundary, in our case a poloidal limiter. In the future we plan to generalize the proof of Tasso, Green, and Zeehrfeld [1] to include nonexistence of a nontrivial *stationary* equilibrium for plasmas with *finite* boundary density and pressure, which explains why the equilibria must be fluctuating. In a recent paper [3] the experimental results reported here are supported by numerical simulations, which also give insight into the global dynamics of the fluctuations and how they can improve the confinement.

The paper is organized as follows. In Sec. II we describe the experimental conditions in the Blaamann device. The fluctuation analysis, the conditional sampling in particular, is discussed in Sec. III, together with a Monte Carlo simulation presented in the Appendix. A cross-parametric analysis, involving signals measuring two different physical quantities, is discussed in Sec. IV, where electron temperature fluctuations are discussed in particular. The fluctuations have also been investigated by a wavelet analysis, with results discussed in Sec. V. This analysis allows information to be extracted directly from a transformed presentation of the raw data, while the first sections were concerned with statistical averages. Finally Sec. VI contains our conclusions. The first results from our study in the Blaamann torus were published by Øynes, Pécseli, and Rypdal [4].

II. STEADY-STATE CONDITIONS

The Blaamann device is a toroidal plasma device with major and minor radii of 651 and 133 mm, respectively. A detailed description of the device is given in Refs. [2,5]. A toroidal magnetic field up to 0.4 T with a ripple ($\delta B/B$) less than 0.01 at the center is generated by 24 coils. The magnetic field system also contains eight horizontally positioned coils, concentric with the major axis. These coils are used for creating auxiliary radial and/or vertical magnetic fields inside the vacuum chamber. For the experiments described in this and the following sections a hydrogen plasma is created by 140 eV electrons emitted from a negatively biased hot tungsten filament. These primary electrons flow in both toroidal directions, subject to vertical ∇B and curvature drifts and poloidal $\mathbf{E}\times\mathbf{B}$ drift, ionizing the neutral gas under constant, monitored pressure. A poloidal limiter extending 2 cm inward from the wall acts as the main anode for the resulting discharge current. There is no transformer action to induce a toroidal electric field, and no externally imposed toroidal electric current, hence there is no poloidal magnetic field except those radial and vertical fields which can be imposed by the auxiliary coils. The results presented in the following refer to hydrogen plasmas, although the device has been operated also with other plasmas, argon, for instance.

The measurements of the time averaged basic parameters shown in Fig. 1 are obtained by using a computer controlled, motor-driven, Langmuir probe with an exposed spherical probe tip of diameter 1 mm. Full Langmuir characteristics were obtained at selected spatial resolution in a cross section of the Blaamann device and the steady-state plasma potential

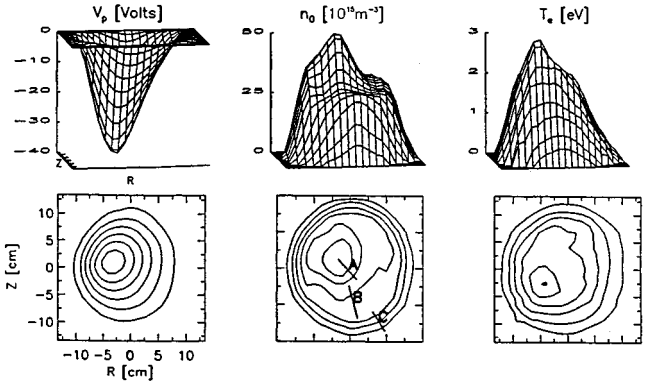

FIG. 1. Plasma potential V_p, density n_0, and electron temperature T_e, for the selected reference plasma parameters. R is the major radius coordinate, and Z is the coordinate along the major axis. The filament is vertical at the position $R=-7$ cm, extending from $Z=8$ to -8 cm, approximately. The axis of the torus is in the negative R direction.

and density are deduced from these. It has been explicitly verified [2] that there is little global perturbation of the plasma by the probe. In Fig. 1 we see plasma potential, electron density, and electron temperature for a selected equilibrium with a toroidal magnetic field, $B_0=110$ mT, vertical magnetic field, $B_z=0.3$ mT, giving an ion cyclotron frequency $\omega_{ci}\approx 10^7$ rad/s. The neutral gas pressure was 8.4×10^{-4} mbar. These parameters are selected here because one obtains a well defined plasma column with closed, almost circular, equipotential contours, indicating that there is little loss to the walls of the confining vessel due to the mean $\mathbf{E}\times\mathbf{B}$ flow. As the following analysis demonstrates, there are nevertheless losses of a ''bursty'' nature due to fluctuations. The parameters may be varied to obtain different fluctuating equilibria [2], and it has been verified that these equilibria are highly reproducible.

To a first approximation the average potential profile can be considered parabolic, i.e., the averaged electric field $\overline{E(r)}$ increases approximately linearly with radius from the local potential minimum. This implies an almost shear-free bulk $\mathbf{E}\times\mathbf{B}$ poloidal plasma rotation velocity $\mathbf{v}_E$. With $\max|V_p|\approx 35$ V, we have the angular poloidal rotation frequency $\Omega\equiv E/rB\approx 4\times10^4$ rad/s, or $\Omega/2\pi\approx 5$ kHz. For comparison we have the estimate $\omega^*/2\pi\approx 1$ kHz for the drift frequency.

The potential well responsible for the poloidal rotation is created by the injection of negative charge through the cathode, and the growth of this well is saturated by a radial current due to a turbulent viscous force in the poloidal direction. As shown by numerical simulations in [3], the fluctuation responsible for this force is the nonlinear stage of an electrostatic Rayleigh-Taylor flute-type instability, driven by the pressure gradient together with the centrifugal force due to the poloidal rotation. Moreover, the simulations indicate that the fluctuating state is also influenced by the driving mechanisms of the curvature-driven interchange instability, which seems to be responsible for the rotating dipole structures which are observed in the simulations as well as in the experiments reported in this paper.

The continuing free energy for the instabilities is derived from the sources in charge and mass, i.e., the injection of

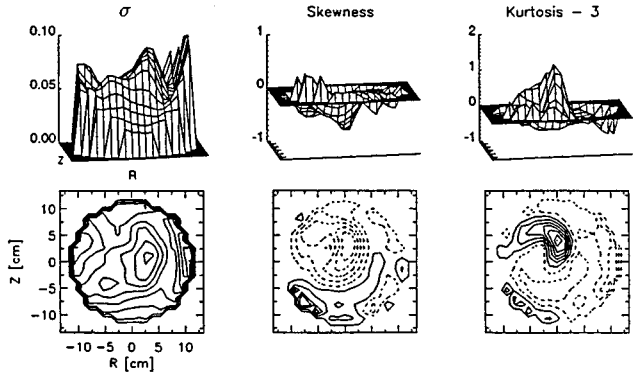

FIG. 2. Spatial variation of standard deviation of the relative density fluctuations, their skewness and kurtosis (where the number 3 characterizing a Gaussian probability density is subtracted). The contour interval is 0.011 for the standard deviation, 0.123 for the skewness, and 0.189 for the kurtosis. These intervals were selected for the sake of presentation. (Our estimates for the relative density fluctuations at the very edge of the plasma column are somewhat uncertain since they are obtained as the ratio of two small numbers.)

electrons and subsequent ionization, which maintain the poloidal rotation and the radial plasma density gradient. This gradient, of course, may also give rise to drift-wave instability, and one cannot exclude the possibility that drift waves coexist with flute modes. It will be shown in this paper, however, that the dominant large scale coherent structures are of the flute type. This is consistent with the simulations in [3], which reproduces the most important features of the experiments from a flute-mode model.

III. FLUCTUATIONS IN PLASMA DENSITY AND POTENTIAL

Fluctuations in potential and density are detected by the same Langmuir probes which were used for the dc measurements. Typical frequencies for the fluctuations are below 10 kHz. For comparison we note that relevant ion cyclotron frequencies are above 1 MHz. A number of signal sequences of typically 4 ms duration are recorded and stored for a subsequent numerical analysis. For the present purpose the sampling rate was chosen to be 100 kHz. The time series in floating potential and electron saturation current all give non-Gaussian amplitude statistics for most of our experiments as evidenced by a nonvanishing skewness S and a kurtosis K deviating from the value 3 which characterizes a Gaussian. The spatial variation of the standard deviation, S, and K, are shown in Fig. 2. Thus, for example, $S=-0.3$, -0.2, 0 and $K=3.0$, 2.8, 3.1 for the three regions A, B, and C in Fig. 1, respectively. Note that the estimate of the relative density fluctuation is uncertain at the edge of the plasma, where we take the ratio of two small numbers, both subject to statistical uncertainty. However, there are statistically significant fluctuation enhancements at positions where the centrifugal force causing the curvature drift is antiparallel with the local density gradient.

The observed fluctuations are random, but in the time series there are some repetitive signatures which can be distinguished from the Gaussian background noise. If we assume these signatures to be caused by, or related to, some propagating localized or intermittent structure in the plasma, the average evolution of such an event can be examined by means of conditional averaging, where, for instance, a standard correlation analysis can provide only little relevant information.

A. Conditional sampling

The conditional sampling and averaging method has been described in [6,7]. We here only give a brief overview of the method and its interpretation, with some details discussed in the Appendix. The method as used in the following is based on a two-probe diagnostic. One probe is kept at a fixed reference position measuring an observable Φ_1, while the other probe scans selected points in a cross section of the plasma column measuring Φ_2. The quantities Φ_1 and Φ_2 can individually represent any observable, such as density, potential, or temperature. We use a condition C defining time windows of selected size centered around a specific signature at the reference probe, for instance, a certain signal amplitude. We define the *conditional time windows* to be the subseries at the movable probe corresponding to a fulfillment of C. At each position of the moving probe we average all acquired conditional time windows, getting the conditional averaged time series

$$\Phi_{\mathrm{CA}}=\langle\Phi_2|C\rangle. \tag{2}$$

In this manner we are able to determine the average time variation of an observable Φ_2 at any location in the plasma centered around an event at a fixed spatial position. By presenting the results of this analysis as contour or surface plots, we can describe the average time evolution of the structures causing, or being correlated with, the signature selected as our triggering condition. The simplest signature to look for is amplitude levels higher than some critical value, either absolute or relative to the average fluctuation level. The ideas are illustrated in more detail in Fig. 3, showing actual data.

While the conditional averaging method gives the space-time evolution of an *average* structure, it does not give any indication of how individual structures deviate from this average. By defining the *conditional variance* (C^{var}) as

$$C^{\mathrm{var}}=\frac{\langle(\Phi_2-\langle\Phi_2|C\rangle)^2|C\rangle}{\langle(\Phi_2|C)^2\rangle}, \tag{3}$$

where $0\leqslant C^{\mathrm{var}}\leqslant 1$, we obtain a measure for the reproducibility of the *entire* event, i.e., the shape and position of a potential structure, and in particular also its trajectory. Small values of C^{var} indicate a high degree of reproducibility, and $C^{\mathrm{var}}\approx 1$ means little or no reproducibility. For representation it might be advantageous to define a *conditional reproducibility* (C^{rep})

$$C^{\mathrm{rep}}\equiv 1-C^{\mathrm{var}}. \tag{4}$$

A conditional variance (or conditional standard deviation) was introduced already in [6] although with a normalization different from the one used in Eq. (3).

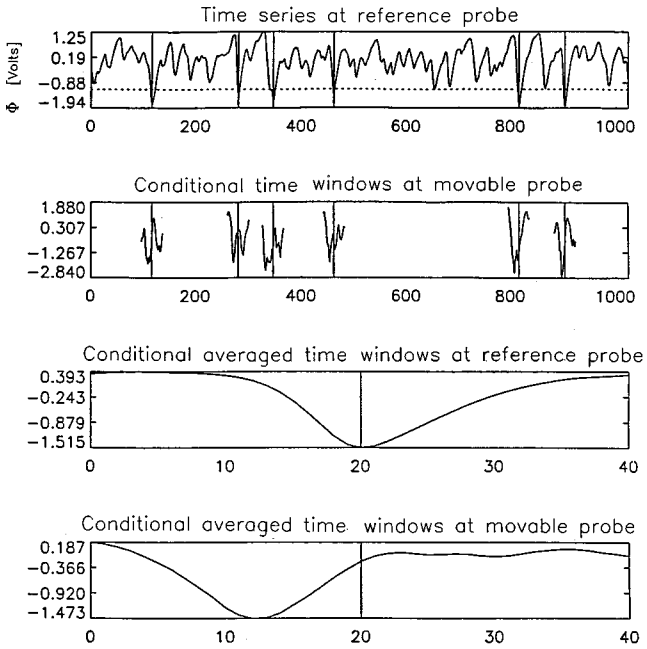

FIG. 3. Illustration of conditional sampling as applied to the present data. Examining a reference signal, top frame, we select times where the signal fulfills a selected condition, in the present case, $\Phi_1 < -2\sigma_1$, where σ_1 is the root mean square of the reference signal. The selection of the exact reference time is here done by locating the next time the signal crosses the reference level, now in the opposite direction, and a conditional time interval between these two times is obtained. The reference time is then placed at the largest local extremum, in the present case the deepest local minimum, within this time interval. Given the reference time, conditional time windows with given duration are selected symmetrically around the reference time in the other signal, here the one from the movable probe, see second frame. The signals from many such time intervals are averaged to give results as shown in the two lower frames.

The conditional analysis is different from a simple correlation. It is thus readily seen that the conditional average is sensitive, for instance, to the sign or polarity of structures, in contrast to a simple correlation which in effect squares the signal and is thus insensitive to a sign reversal. The relation between the conditional analysis and correlation functions in studies of electrostatic turbulence has been discussed in, e.g., [8].

Conditional sampling has been applied in a number of other experiments, for instance, also in the Texas Experimental Tokamak Upgrade (TEXT-U) [9], but the results are not in all cases supporting a model with large coherent structures being present in the turbulence. The simplest interpretation is of course that *no* such structures are present, and indeed in the case where the turbulent fluctuations constitute a Gaussian random process no such structures can be identified [8]. However, in some cases it is the conditional sampling method which imposes some restriction on the interpretation, and in the Appendix we illustrate such a case by a Monte Carlo simulation, using a synthetic signal. In particular, we there also illustrate the performance of a conditional analysis as compared to a simple correlation between the reference signal and the one obtained from the moving probe.

B. Basic results

For the selected plasma parameters specified before, we have performed a conditional averaging experiment measuring density fluctuations (obtained by the electron saturation current) on both probes with the results shown in Fig. 4. The fluctuations in density are here normalized in each spatial position by the local average density. The condition used for triggering was in this case

$$\Phi_1 < -1.5\sigma_1, \tag{5}$$

where σ_1 is the root mean square associated with the time series from the reference probe. Here, $\sigma_1 = 7 \times 10^{-2}$ in terms of the relative density fluctuations. The different frames in Figs. 4 and 5 are obtained by numerical interpolation of measurements performed for probe positions on a grid marked by dots in the figures for $\tau = 0$. The analysis reveals the formation and propagation of a dipole shaped structure transforming into a monopole while it rotates in $\mathbf{E} \times \mathbf{B}$ direction around the density peak shown in the equilibrium measurements. The figures show the fluctuating quantities only. These are to be superimposed on the dc variations shown in Fig. 1.

We also calculated the conditional reproducibility given by Eq. (4) and found that the trajectories and the extremum values of the structures are highly reproducible, see Fig. 4(b). The statistical uncertainty of the result increases away from the extremum value. At present we cannot distinguish whether this uncertainty represents variations in the structures from one realization to another, or being alternatively a signature of a ''flapping'' of the edges of the structure as it propagates.

Similar results have been obtained for a wide range of plasma parameters. The signals of the conditionally selected subseries have significantly non-Gaussian characteristics, and the forms and time variations of the conditionally averaged structures depend significantly on the imposed conditions, in particular, their polarity. In cases where large structures appear seldom, they *need* not give rise to significantly non-Gaussian amplitude distributions for the *entire* time records in the regions where they occur. In the present case, however, even the unconditionally analyzed time series are non-Gaussian, as evidenced by the skewness and kurtosis values shown in Fig. 2.

The large coherent structures are expected to be important for particle transport across magnetic field lines. Charged particles are propagating essentially with the local $\mathbf{E} \times \mathbf{B}/B^2$ velocity along equipotential contours, which have the role of streamlines. The potential *perturbations* observed by the conditional averaging method correspond approximately to the conditionally averaged potential in the rotating frame of reference moving with the average plasma flow. Hence the level curves for this potential constitute flow surfaces for the plasma in this frame of reference during the lifetime of a structure. If the lifetime of a dipole structure is comparable to the rotation time of each vortex in the dipole, the plasma will be transported radially a distance comparable to the vortex size during this time. The transport can of course be substantial even if the lifetime of the structures is shorter, the plasma lifetime will then just be longer than the vortex time. It may be appropriate here to emphasize that the time scales and lifetimes deduced from conditional averages should not

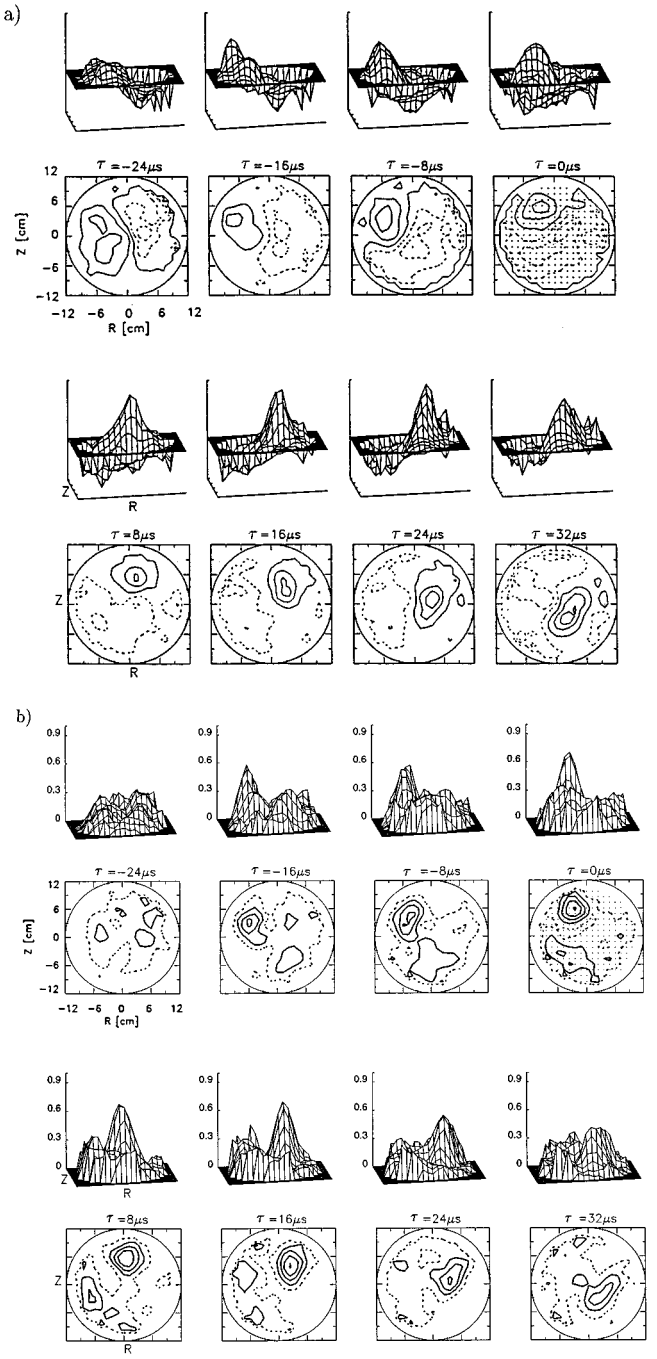

FIG. 4. Temporal variation of the conditionally averaged local relative density fluctuations is shown in (a) as obtained with the reference probe in the position $(R,Z)=(-2.85, 5.0)$ cm, at the same toroidal position as the movable probe. τ is the relative time for triggering, i.e., $\tau=0$ corresponds to the time of the triggering event at reference probe. The toroidal magnetic field is into the paper plane. Solid lines denote positive contours, dotted lines negative ones. The separation between contours corresponds to 3% relative density fluctuations. The range of R-Z variations given here applies to the following figures as well. The small dots at the frame for zero time delay indicate the spatial positions where the analysis was carried out, the contours being obtained by numerical interpolation to give the full figures. In (b) we show the conditional reproducibility obtained for the analysis in (a).

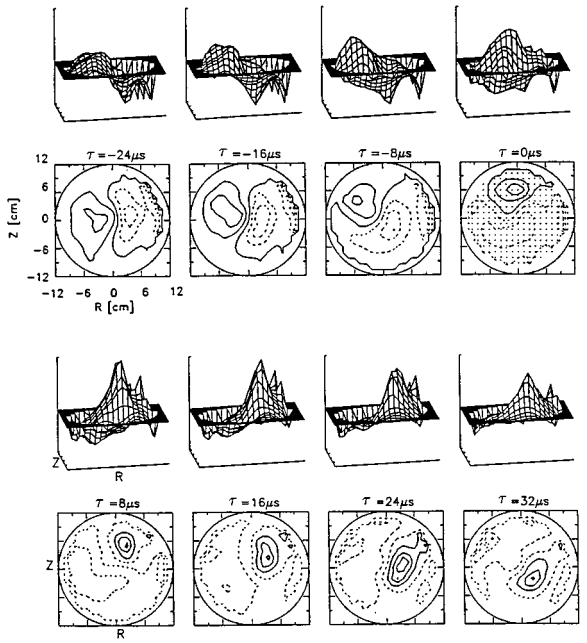

FIG. 5. Conditional averaging with reference probe displaced 90° toroidally relative to the movable probe. We used the same triggering condition and contour separations as in Fig. 4(a).

be confused with characteristics of *individual* structures. This particular question is discussed in some detail in [10]. Here we only mention that in general one will expect lifetimes of individual structures to be comparable to or *larger* than what is deduced from the conditional average.

To get an indication on whether the driving force is drift-mode or flute-mode instabilities, we repeated the conditional averaging experiment with the reference probe displaced 90° toroidally relative to the previous experiment with the results shown in Fig. 5. Since drift-mode waves have a finite **B**-parallel wavelength, while flute modes are strictly parallel to the magnetic field lines, we would expect to see a ''phase shift'' between the two experiments in the case of drift modes but not for flute modes. By comparing Figs. 4(a) and 5 we find no such phase shift, indicating flute-mode instabilities.

The identification of flute modes in the present toroidal plasma is unambiguous, in contrast to the results in the linear Q device discussed in, e.g., [10], where end-plate conditions can accommodate a phase shift [11], which can be measured only with limited accuracy. Moreover, the drift-mode scaling implies $e\Phi/\kappa T_e \approx \delta n/n_0$, which is in disagreement with our observations. We find $e\Phi/\kappa T_e \approx -3\,\delta n/n_0$ as an additional support for the interpretation in terms of flute modes. Due to the uncertainty introduced by the high bulk plasma rotation velocity, it is not possible to give an accurate estimate for velocity of the structures in the rest frame of the plasma.

We note that the characteristic of the Langmuir probe is inclined in the electron saturation region also in our experiment (i.e., the probe characteristic does not actually saturate in the ''electron saturation'' regime). In order to ensure that the observed fluctuations in what we interpret as electron saturation current are not misinterpreted due to fluctuations in plasma potential with a corresponding displacement of the entire characteristic, we repeated the density fluctuation mea-

surements by detecting the ion saturation current with a floating double probe with a fixed bias between the probe tips. The results were similar to those above, possibly with even smaller values of $|\delta n/n_0|$. In the measurements described in this section we find a density depletion to have a surplus of positive charge, which is not consistent with drift waves but indicates flutelike convective cells. The implications of the arguments outlined here are that the observed structures are not wavelike modes, but some where particles are carried along with the structures in a vortical motion.

The Rayleigh-Taylor instability induced by magnetic field curvature has been suggested as a possible source for the excitation of such fluctuations in this type of device [12], and the localized mode evident in Fig. 2 is consistent with such an interpretation. We emphasize, though, that the analysis of this paper should be applied with care as it refers to perturbations of an equilibrium condition which in the strict sense does not exist in Blaamann or similar devices, as already mentioned. The simulations in [3] also show that results from linear stability analysis should be applied with caution, since the ''equilibrium'' is actually a strongly fluctuating, driven state.

C. Spatial distribution of structures

A local measure of the relative weight of the large amplitude structures compared to the background turbulence can be obtained by a conditional analysis of the signal from the movable probe itself. For this purpose we select a certain length for the time series (here 4096 μs) and count the number of times per second, N_c, that the signal exceeds a value $c\sigma$, where c is a variable coefficient and $\sigma=\sigma(R,Z)$ is now the *local* standard deviation for the signal in the actual position of the movable probe. The value of N_c can then be plotted as a function of c for a given position. The curve is evidently monotonically decreasing. Examples are shown in Fig. 6(a) for the selected probe positions corresponding to the centers of regions A, B, and C in Fig. 1. The higher counts in region B indicate that the large coherent structures have a more dominant role in the turbulence in this region. Similar information is obtained in Fig. 6(b) where N_c is plotted as a function of spatial coordinates for $c=1.5$. The annular region of maximum counts coincides with region B, and corresponds to the trajectory of the peak amplitude of the conditionally averaged signal, which can be found from Fig. 4. From Fig. 1 it can also be seen that region B has a smaller density gradient than regions A and C. This is displayed even more clearly in Figs. 6(c) and 6(d), where vertical and horizontal profiles of N_c (for $c=1.5$) and n are plotted. The density gradient is flattened in regions where the turbulence is dominated by the large amplitude structures (i.e., where N_c is large). Assuming that all of the plasma is produced in the vicinity of the filament [2] we can argue that the radial plasma flux is independent of distance from the filament. The anomalous plasma diffusion coefficient will consequently be inversely proportional to the density gradient. This means that the diffusion coefficient is higher in the region dominated by the coherent structures. It is therefore plausible that these structures have a significant role in enhancing the radial plasma transport. Independent experiments in our device based on three-probe measurements of

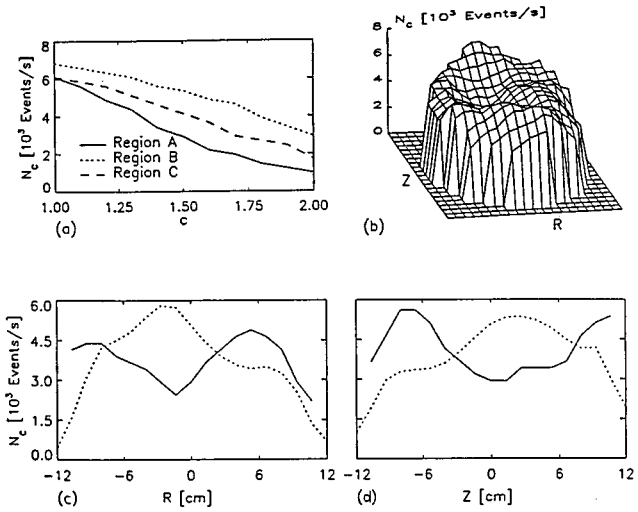

FIG. 6. The number of times per second, N_c, that the signal of the movable probe exceeds $c\sigma$ is shown as a function of c for three different spatial positions (a). In (b) we show N_c as a function of (R,Z) for $c=1.5$. In (c) N_c is shown with solid line as a function of R for $Z=0$ and $c=1.5$, while in (b) N_c is shown as a function of Z for $R=0$ and $c=1.5$. The average density variation is shown with a dotted line for both cases, see Fig. 1.

the fluctuating electron temperature confirm that the large scale structures give rise to outward bursts of hot electrons originating from the filament region.

Inspection of the temperature profile in Fig. 1 shows that it is similar to the density profile. The maximum value is shifted somewhat downwards as a consequence of the larger downwards curvature drift of the high-energy population of electrons. The flat density profile in region B in Fig. 1 can then consistently be viewed as a consequence of the strong ''stirring'' of the plasma in this region due to the vortex motion.

IV. CROSS-PARAMETRIC CONDITIONAL ANALYSIS

To provide a detailed analysis of the fluctuations in the Blaamann device we also performed a *cross-parametric* conditional analysis, by using the signal for one physical parameter (e.g., temperature) as reference and another (e.g., density) as the conditionally averaged signal. By proper choice of reference signal it is possible to distinguish different phenomena in the *same* data set [13].

We performed the following analysis combining different signals. First, with the reference probe detecting fluctuations in potential, we made a conditional analysis of fluctuations in density and potential as detected by the movable probe. Then, using the fluctuating electron temperature as reference, we again made a conditional analysis of fluctuating density and fluctuating potential as detected by a movable probe.

In order to demonstrate that the phenomena discussed in this study are not referring to one particular set of parameters only, we selected a set of basic reference parameters differing from that in Fig. 1; a hydrogen plasma in a toroidal magnetic field of 88 mT, vertical magnetic field 0.24 mT, and neutral gas pressure 3.8×10^{-4} mbar, implying a reduced collisionality with neutrals as compared with the conditions in Fig. 1. The direction of the magnetic field was also

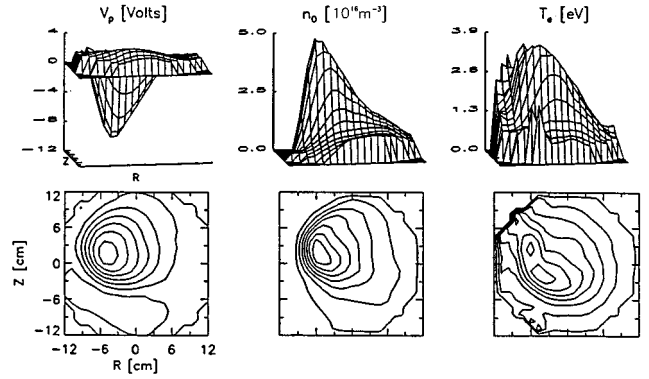

FIG. 7. Steady-state plasma parameters for study of cross-parametric conditional analysis. The figure shows the plasma potential V_p, density n_0, and electron temperature T_e.

reversed to test whether this parameter was of relevance. The steady-state conditions for these parameters are shown in Fig. 7. Again we observe that the equipotential contour forms closed lines around a local minimum in the vicinity of the hot filament. Fluctuation spectra for these conditions are shown in Fig. 8.

A. Fluctuations in electron temperature

Fluctuations in electron temperature were detected by a triple probe [14]. The three probes were placed in triangular positions at a relative distance of 5 mm. For the present purpose we had two of the probes connected in a double-probe configuration with a constant relative bias of 9 V. The electron temperature T_e is expressed in terms of the floating potentials of the single probe, V_{SP}, and of the positively biased one of the double probes, V_{DP},

$$T_e = \frac{V_{\mathrm{DP}} - V_{\mathrm{SP}}}{\ln 2}. \tag{6}$$

This simple expression implicitly assumes that the electrons are characterized by a Maxwellian distribution. This assumption does not hold close to the filament, and we therefore only used the triple probe for electron temperature measurements at spatial positions well separated from the filament region. The plasma density fluctuations can be detected simultaneously from the current fluctuations to the double probe. The time resolution of the probe potential, and thus the electron temperature, was 0.2 ms, and ideally we are able to resolve fluctuations in temperature on the same time scale as the variations in potential and plasma density. Power spectra of the fluctuations in electron temperature are shown in Fig. 8(b).

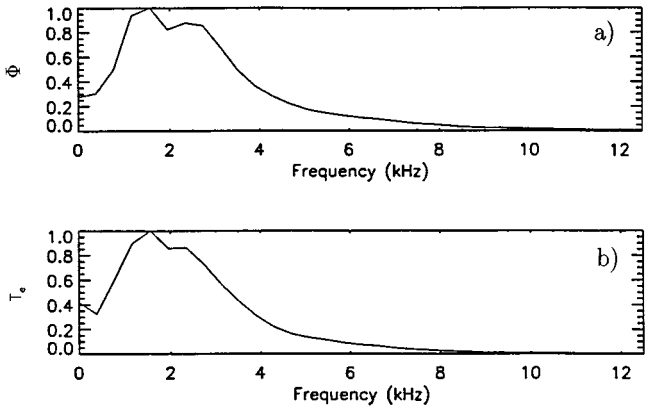

FIG. 8. Power spectra (in arbitrary units) for (a) fluctuations in floating potential, and (b) fluctuations in electron temperature.

We found that the power spectra for fluctuations in density and electron temperature appeared rather similar, indicating that a warm electron component can be considered as a constituent which here, at least approximately, passively follows the plasma flow and therefore has the same fluctuation characteristics. This question will be addressed again later on by investigating the phase relations between the fluctuations in electron temperature, plasma density, and potential, respectively.

B. Potential fluctuations as reference

The reference probe was placed in the position $(R,Z) = (2,0)$ cm at the same toroidal position as the movable probe. Results are shown in Fig. 9, where (a) is referring to the case where the movable probe detects potential, while in (b) it was detecting density fluctuations. In this case the density fluctuations are *not* normalized by the local average density, and the results in (b) are shown in arbitrary units. The imposed condition was $\Phi_1 < -1.5\sigma_\phi$ in both cases, where σ_ϕ is the standard deviation for the potential fluctuations. The imposed condition was varied, taking also $\Phi_1 > 1.5\sigma_\phi$, for instance. Also the conditional reproducibility, as defined before, was obtained. A typical result is shown in Fig. 10 for the case where the movable probe detects potential fluctuations. There is a tendency for the conditional reproducibility to increase somewhat slower towards the reference time, $\tau < 0$, compared to the time scale for its decrease at increasing times, $\tau > 0$.

C. Fluctuating electron temperature as reference

In this case we use the triple probe detecting fluctuations in electron temperature as the reference probe. The triple probe was also placed in the position $(R,Z) = (2,0)$ cm, at the same toroidal position as the movable probe. At this position the fast electron component is negligible and the assumption of Maxwellian distribution implied in the interpretation of the probe signal is well satisfied. Typical results are shown in Fig. 11, where (a) refers to the case where the movable probe detects potential, while in (b) it was detecting density fluctuations. The imposed condition was $\Phi_1 < -1.5\sigma_{T_e}$ in both cases, where σ_{T_e} is the standard deviation for the temperature fluctuations. The imposed condition was varied, taking also $\Phi_1 > 1.5\sigma_{T_e}$, for instance. Also the conditional reproducibility was obtained. Qualitatively, these results were similar to those shown for the other conditional reproducibilities.

D. Temporal distribution of events

The peaks in the spectra shown in Fig. 8 demonstrate that there is well defined periodicity associated with the signals. It is, however, not *a priori* obvious what relation this peri-

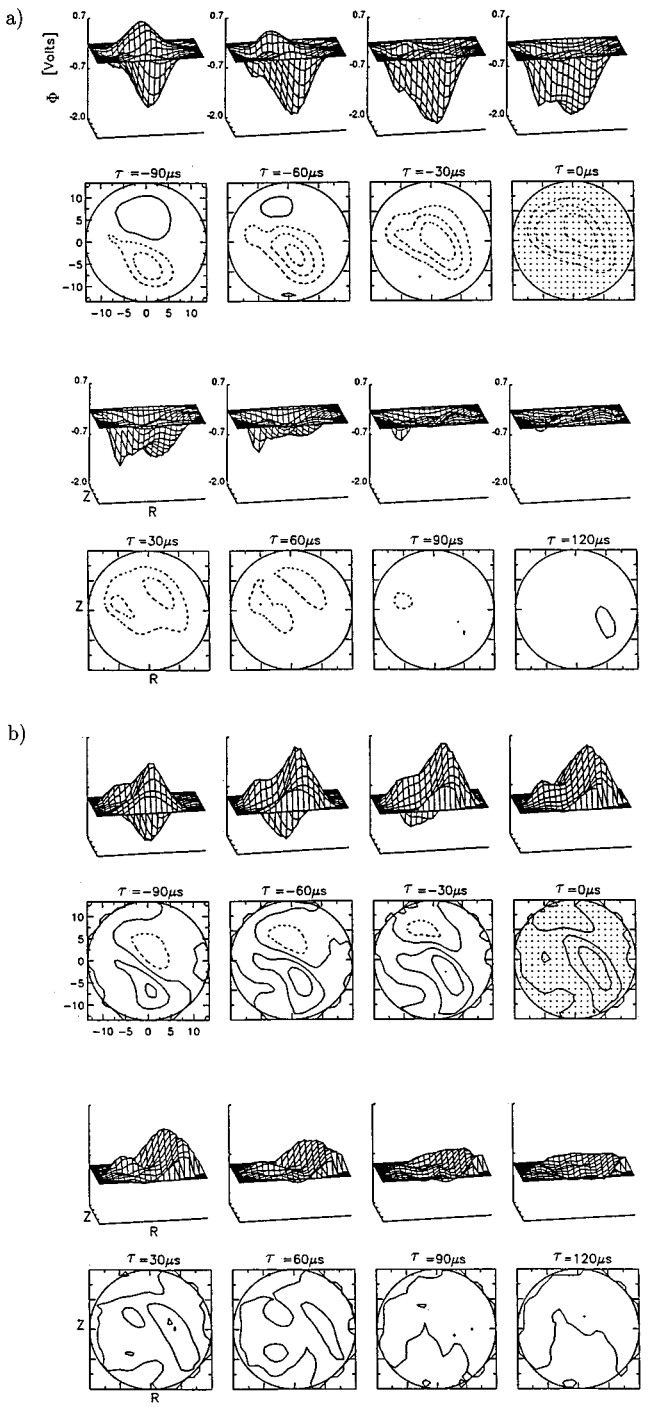

FIG. 9. Conditional average where a condition is imposed on the reference signal for fluctuations in potential, where (a) is referring to the case where the movable probe detects potential, while in (b) it was detecting density fluctuations. The results in (b) are given in arbitrary units. The imposed condition was $\Phi_1 < -1.5\sigma_\phi$ in both cases. The reference probe was in the position $(R,Z)=(2,0)$ cm.

odicity has to the observed conditional structures. To study this particular question we performed a time-delay analysis. This was carried out by forming a histogram of the time delay between consecutive events detected by the reference probe. A set of 3050 time series, each of 1024 sample points, were collected, forming a total of ~ 31 s. The time delay between two successive fulfillments of the condition

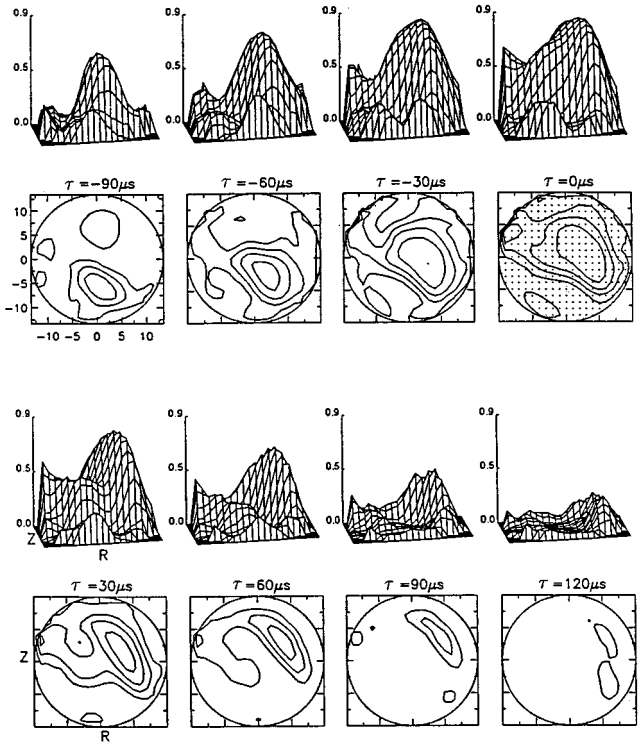

FIG. 10. Conditional reproducibility as defined in Eqs. (3) and (4) for the case where both the reference probe and the movable probe detect fluctuations in potential. The imposed condition is as in Fig. 9(a).

$\Phi_1 < c\sigma$ was recorded for negative values of the c with $c=-(1+0.25n)$ where $n \in \{0,...,6\}$. Again Φ_1 denotes the measured quantity, i.e., fluctuations in potential or electron temperature. Quite similarly we can study positive values of c by $\Phi_1 > c\sigma$. Results are shown in Fig. 12(a) for the case where the reference probe detects potential fluctuations. The sharp drop in the distribution at short time delays is introduced by the selection window, which in this case has a half-width of 200 μs; the windows are nonoverlapping. The time resolution was in this case 20 μs.

In a quite similar manner we can analyze the case where the reference signal comes from the triple probe detecting fluctuations in electron temperature. Results are shown in Fig. 12(b), again for the positive polarity of the imposed condition. Also the negative polarities were investigated, giving slightly different results, which can be explained by the difference in signal-amplitude probability density for the two polarities.

E. Discussion

The main features of the experimental results described before can be summarized as follows. The formation and propagation and decay of large structures can be observed, and the direction of propagation along the $\mathbf{E}\times\mathbf{B}$ drift, the dc electric field $\mathbf{E}$ being derived from the potential distribution shown in Fig. 7. The velocity of propagation is of the same order of magnitude as the $\mathbf{E}\times\mathbf{B}/B^2$ velocity. The time scales for the formation and for the decay are different; we find that in general a structure decays on a time much faster than the one on which it is being formed. In particular, the condi-

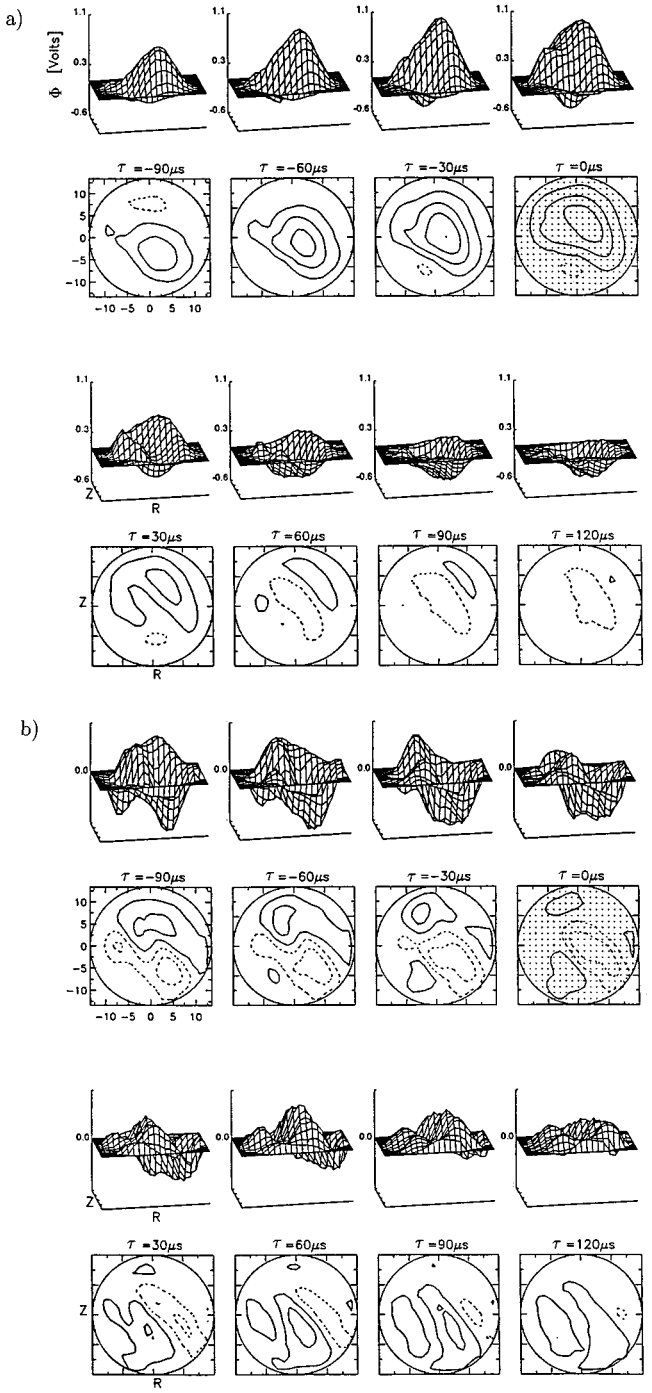

FIG. 11. Conditional average where a condition is imposed on the reference signal for electron temperature fluctuations, where (a) refers to the case where the movable probe detects potential, while in (b) it was detecting density fluctuations. The results in (b) are given in arbitrary units. The imposed condition was $\Phi_1 < -1.5\sigma_{T_e}$ in both cases. The reference probe was in the position $(R,Z)=(2,0)$ cm.

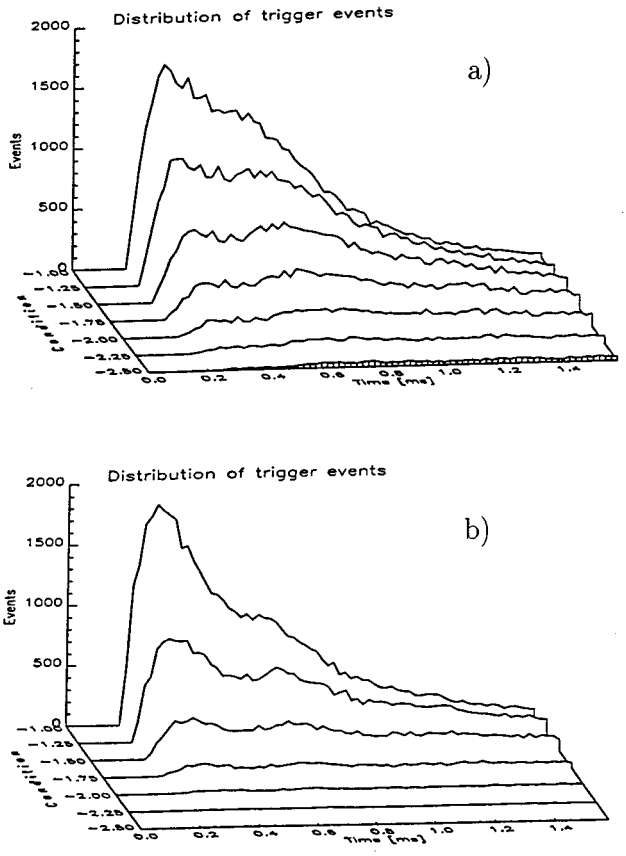

FIG. 12. Normalized distribution of time delays for different values of c as a function of time for positive values of c. The condition is in (a) imposed on the signal measuring fluctuations in potential, in (b) on the signal measuring fluctuations in electron temperature. The resolution, i.e., the bin size of the histogram, is 20 μs.

tional reproducibility analysis shown in Fig. 10 indicates that the structures all grow more or less at the same rate, since C^{var} as defined by Eqs. (3) and (4) varies only little during the growth phase. The decay phase is apparently more irregular, with C^{var} decaying within half the growth time. It is important to emphasize that what is here interpreted as lifetime for structures is not necessarily to be interpreted as the time it takes a structure to decay to a small amplitude, rather and more generally it is the time it takes it to be deformed so much that its shape has lost any statistical relation to its original form [10]. In the simulations by Rypdal, Garcia, and Paulsen [3] it is observed that the dipole vortex structures are destroyed in events which lead to bursts of anomalous radial charge transport, and hence to some reduction in the depth of the potential well, and this happens more quickly and in a more erratic way than the more gradual buildup of the structures. Moreover, the time scales of these processes are very close to what is observed here. Thus it seems quite plausible that the two-dimensional flute-mode model, on which these simulations are based, provides an adequate description of the global dynamics of this system.

The size of the structures seems to be determined by the geometry of the plasma in the cross section of the column, i.e., the overall radial scale of the conditionally averaged structures seems to be the column radius irrespective of which signal was used for reference.

Considering the frame for vanishing time delay, $\tau=0$, in Fig. 9(b) we find that density and potential are in antiphase, in agreement also with the results in Sec. III and the simulations in [3]. This means that when the imposed condition on the potential at the reference probe is negative (as in Fig. 9), we find a positive value for the conditionally averaged

density, and demonstrates again that the structures are unlikely to be drift-wave type. The conclusions were confirmed by investigating both polarities of the imposed condition. The internal phase relations between the signals could be obtained by a correlation analysis as well, and have been confirmed explicitly by performing the relevant estimates.

Considering the frame for vanishing time delay, $\tau=0$, in Fig. 11(b) we find that density and electron temperature are in phase, i.e., when the imposed condition on the electron temperature at the reference probe is negative (as in Fig. 11), we find a negative value for the conditionally averaged density, i.e., a density depletion. This result was verified also by repeating the measurement with the opposite polarity on the imposed condition. Since the fluctuating density and potential were in antiphase we can conclude that also the fluctuating electron temperature is in antiphase with potential. This phase relation indicates that a warm electron component is carried with the enhancement of plasma density as it propagates in the azimuthal direction away from the hot filament region. The argument does not necessarily imply that the fluctuations are generated in the filament region.

The observations discussed here are consistent with the picture established earlier, where structures like those in, e.g., Figs. 9 and 11 are not considered as wavelike modes, but rather as perturbations in density, temperature, and potential appearing as dipole vortices drifting along with the mean plasma flow.

Inspection of the time-delay analysis, Fig. 12, shows that there are two characteristic delays, both with a significant scatter. The origin of these two peaks can be explained from the power spectrum in Fig. 8, where also two broad peaks can be observed around 1.5 and 2.5 kHz, the lowest frequency having the largest power. These two frequencies are not harmonically related and it is therefore reasonable to assume that they correspond to two different perturbations, simultaneously present, rather than being the spectral components of *one* irregular rotating structure. Indeed, the inverse time delay for the two maxima in Fig. 12 reproduces the central frequency for the two peaks in the power spectra in Fig. 8 quite well.

From Fig. 12 we conclude that sometimes it is one, sometimes the other component of the fluctuations which fulfills the imposed condition. For small reference amplitudes it is usually the one with the smallest time delay, i.e., the largest frequency in the spectra, Fig. 8, which is observed. As the reference amplitude is increased, it is more and more often the one with the smallest frequency which appears in the time-delay analysis. Note that this discussion has only indirect relevance for the spectral amplitudes in Fig. 8. The magnitude of the peak in the power spectrum is determined by the average amplitude of the appropriate spectral component; this amplitude will usually vary, and this variation is contributing to the width of the appropriate spectral peak.

We have analyzed the data discussed in this section also by a filtering followed by our standard conditional analysis. Bandpass filtering the data for floating potential from the movable as well as the reference probe for the frequency interval {1 kHz; 2 kHz} we find that the oscillations in this interval have the form of a relatively slow deepening of the potential well, followed by a somewhat faster rise in potential across the entire plasma column. If, on the other hand, the signal is bandpass filtered in the interval {2 kHz; 3 kHz}, the same type of investigation shows a propagating dipole-like structure, see Fig. 13. When added to the dc potential, this structure corresponds to a ''tilting'' of the entire potential well. Our observations are consistent with those reported in [15], showing that the frequency spectrum at the bottom of the potential well peaked at a lower frequency than closer to the wall, indicating the existence of fluctuations in the potential well depth, in addition to the fluctuations at somewhat higher frequency due to the rotating dipole structure. Very similar features are also observed in the simulations by Rypdal, Garcia, and Paulsen [3].

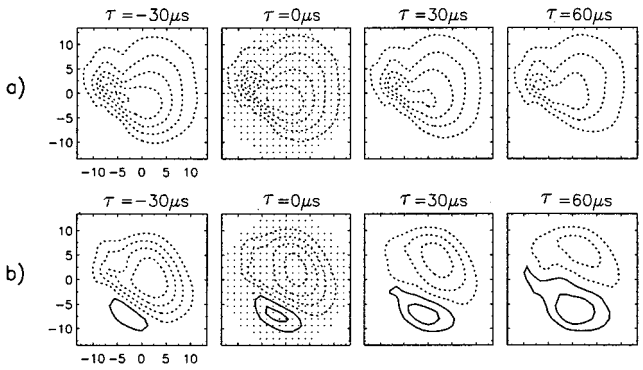

FIG. 13. Conditional analysis of filtered potential fluctuations. (a) shows data obtained after bandpass filtering both signal and reference for {1 kHz; 2 kHz}, (b) filtering for {2 kHz; 3 kHz}. The contour separation is 0.23 and 0.19 V in (a) and (b), respectively.

The bandpass filtering method reported here is valuable for the interpretation of the nature of the fluctuations, but evidently it is not logically possible completely to separate one or the other type of phenomena by this method, since their spectral contents are in general overlapping.

V. WAVELET ANALYSIS

The analysis and discussion presented so far were based on an averaged presentation of the data, and the results are not easily obtained by simple inspection of raw data. Complementary insight, however, can be obtained by finding a representation of the original data which allows direct inspection. We found that some details of the properties of the fluctuations can be understood by considering a wavelet transform of the original signal [16]. This method does not actually comprise data *reduction*. On the contrary, the data sequence with time as one independent variable is now replaced by a representation with two independent variables, time and frequency, implying a large redundancy in the representation. The advantage is a possibility for studying, for instance, variations in the local dominant frequency.

Results from our analysis are illustrated in Fig. 14, obtained for signals recorded simultaneously in two spatial positions. The conclusions from this and similar figures for other combinations of probe positions (at the same plasma parameters) are that the two frequency components around 1.5 and 2.5 kHz are not necessarily present simultaneously. Also the frequencies are not constant, for instance, in Fig. 14 a slight slanting upshift of the 2.5 kHz signal can be noticed. These two observations are consistent with the spectra in

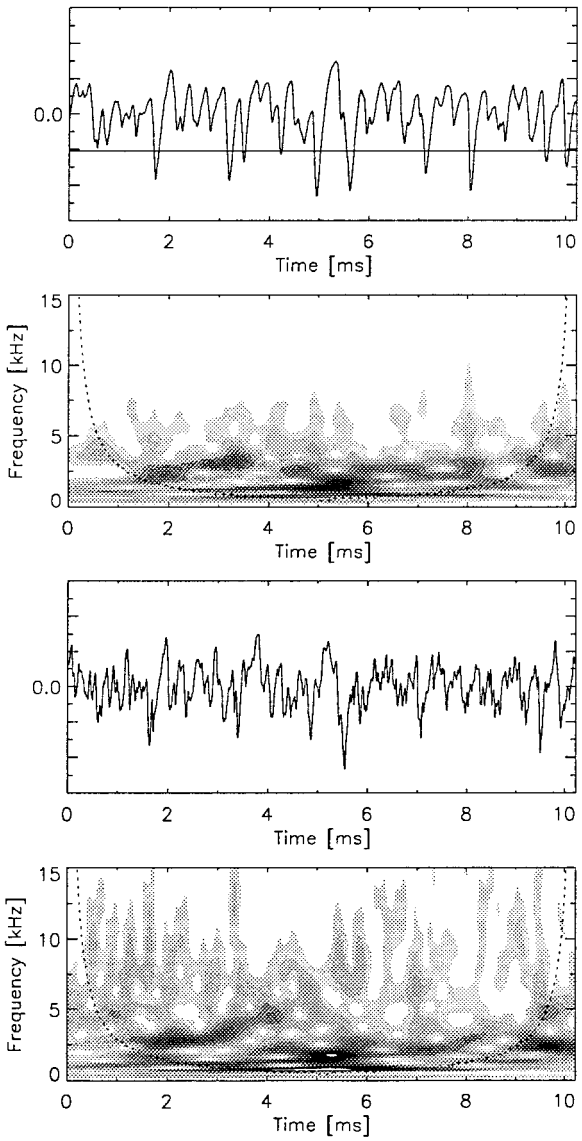

FIG. 14. Wavelet analysis of data sequences. In the top sequence we show data from the reference probe with raw data and wavelet transform, below data from the movable probe placed in the bottom position at $(R,Z)=(0,-4)$ cm. The lowest signal levels are white. The figure is obtained using a transformation based on Morlet's wavelet. The part of the figure below the dashed line is nontrivially influenced by edge effects.

Fig. 8 and also the time-delay analysis in Fig. 12. The linewidth of the power spectra can partly be explained by the shifting frequencies. The time-delay analysis will in short time sequences resolve sometimes one, sometimes the other one of the frequency components as its amplitude varies, as already mentioned. The reason for the frequency drift is likely to be the slow variation in the depth of the entire potential well in, e.g., Fig. 1. The resulting modulation of the $\mathbf{E}\times\mathbf{B}$ rotation of the plasma is consistent with a temporally varying frequency of the high-frequency (~ 2.5 kHz) component, as it is resolved by the wavelet analysis. A frequency drift of, for instance, 500 Hz, requires a variation of approximately 10% in the local minimum of the potential well, which is compatible with observations. Note that this variation is not caused by the ~ 1 kHz signal but is associated with lower frequencies. We have not found evidence for any regularity in the lengths of frequency ''bursts,'' and indeed such a regularity would have given rise to sidebands in the power spectra.

It is noted that no obvious systematic variation of the spectral characteristics can be discerned by visual inspection. It is plausible that the high-frequency part of the spectrum has systematic variations with positions inside or close to a large coherent structure as compared to regions where no structures are present. This question deserves and requires a special analysis which will be addressed in a different context.

VI. CONCLUSIONS

In the present study we analyzed fluctuations in a toroidal device without rotational transform, using a conditional analysis technique. The results demonstrate that the fluctuations are flute type and with a scale size apparently determined by the overall radial scale length of the density variation in the plasma column. The structures do not seem to have any inherent propagation velocity, they seem rather to be transported by the bulk $\mathbf{E}\times\mathbf{B}$ flow in the azimuthal direction. The lifetimes of the structures are comparable to the time of one full azimuthal rotation of the column. Strong indications of the ability of the fluctuations to transport plasma particles were obtained by considering, for instance, the fluctuating electron temperature as a reference signal. The observed structures exhibit spatial as well as temporal intermittency, being localized in space (see, for instance, Figs. 4 and 5) as well as in time (best illustrated in Fig. 12).

We find the overall similarity between the present results and those reported in Refs. [17,18] interesting. The latter experiments were performed in a linear device in a thermally produced plasma. The presence of large vortexlike structures in both experiments indicates that such structures might have some universal properties, and thus be important also, for instance, for confinement in tokamaks or stellerators, the so-called L-H transition, in particular. Coherent structures have also recently been observed in a toroidal magnetic confinement device [19]. This and similar studies rely on a biorthogonal decomposition [20] based on the information obtained simultaneously from a large number of spatially distributed detectors or probes. Coherent structures are by this method identified by a constant spatial form, multiplied in each point by a temporally varying function accounting for the time evolution. A biorthogonal decomposition is thus inadequate in representing structures which deform during their temporal evolution. The two-probe method used in the present work does not have this shortcoming. The biorthogonal decomposition is a fruitful, unbiased method of analyzing and presenting the information contained in a data set, but the standard applications of the method seem to lack a systematic approach to the reduction of the full information inherent in the data.

The experimental observations reported in this work support the essential results from numerical simulations of a one-fluid model for the plasma in the Blaamann device as discussed by Rypdal, Garcia, and Paulsen [3]. Also these results show the formation and propagation of large structures. The model seems to predict that the large scale struc-

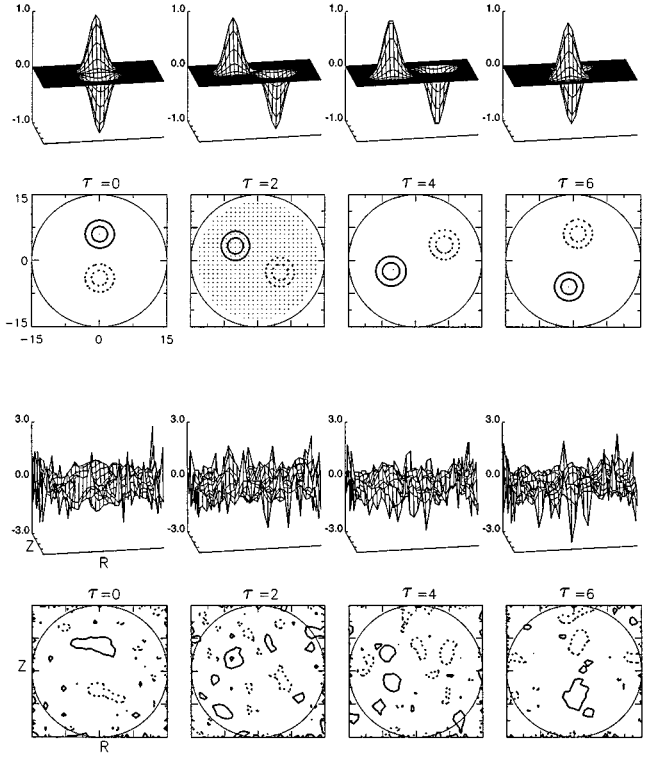

FIG. 15. Illustration of a realization of a synthetic signal in two spatial dimensions for different time steps. The top figure shows two propagating structures with unit amplitudes of opposite polarity and time-varying amplitudes. The bottom figure shows the *same* signal after addition of spatially uniform random noise with zero average and a standard deviation of three units. Space and time are here measured in dimensionless computational units.

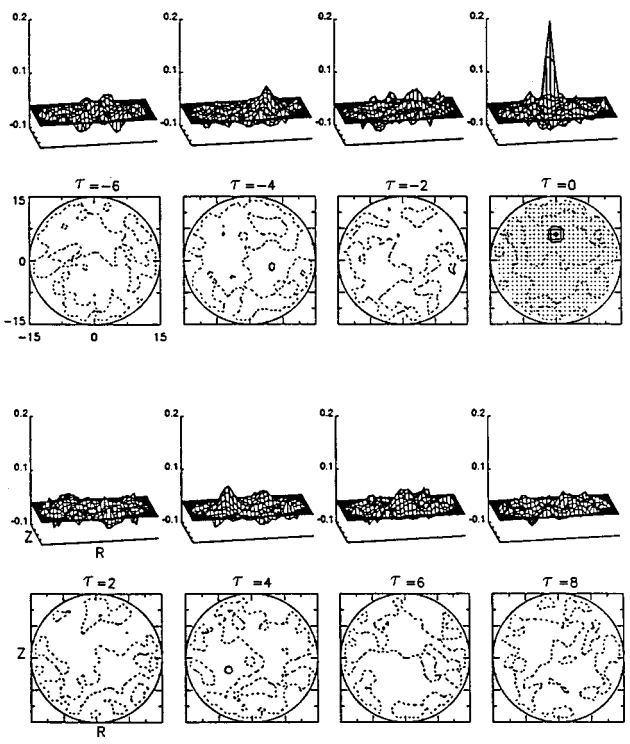

FIG. 16. Correlation analysis of synthetic signal. The cross correlation is obtained for the reference signal obtained at $(R,Z)=(0,6)$ and the signal from each grid point. Space and time are here measured in dimensionless computational units.

tures are directly excited and not a result of a coalescence of smaller scale perturbations as argued for the observations in the linear device [10,21]. An important question remains which concerns the polarity of the observed structures: In the present experimental conditions no significant preference for the polarity of a vortex was found. If the signals were analyzed with the sign of the imposed condition changed, we still observed large coherent structures being formed, although with nontrivial deviations in details of form and propagation characteristics. On the other hand, for a wide range of parameters, the experiments reported in [10,17,22] show a pronounced preference for one polarity of structures. The numerical simulations in [3] indicate a stronger positive density (negative potential) pole, compared to the negative density (positive potential) pole. We find it likely that this apparent controversy can be resolved by a combination of analytical and numerical studies, and coordinated numerical and laboratory experiments. Such a study is now in progress.

In conclusion, we should like to point out some extensions of investigations like those discussed in the present work, where we used rather simple conditions imposed on the reference signal. These can evidently be generalized by imposing conditions not just on the signal level and the sign of its time derivative, but also on second, third, etc. derivatives. Also it might be an advantage in some cases to use, for instance, the time derivative of a signal as reference, rather than the signal itself. It may, however, be more interesting to devise an alternative method where we search for a certain structure or pulse *shape* in the reference signal, assuming that such a pulse shape is given by *a priori* knowledge, theoretical investigations, for instance. The most convenient way of performing such an investigation is to devise a matched filter for the pulse shape in question; assume that a pulse with time variation $f(t)$ is expected to be present in the reference signal. Under fairly general conditions [23], the optimum filter has the impulse characteristic $h(t)=kf(-t)$ where k is an arbitrary constant. The filtered signal $s(t)=\int_{-\infty}^{\infty}\Phi(\tau)h(t-\tau)d\tau$ is thus designed to have large value at the time where the pulse is present in the signal, but being relatively small otherwise. This filtered signal can then be used for a conditional analysis similar to the one carried out in the present study. The condition is now to be imposed on the signal $s(t)$, by, for instance, requiring $s(t)$ to have a local maximum above a certain level at the reference time in the selected subinterval. The signal from another probe can then be analyzed as before.

The ideas outlined here are expected to be particularly relevant in cases where coherent structures characterized by analytical expressions, possibly containing a set of parameters, are derived analytically, double vortices in drift-wave turbulence being one example. In such cases a matched filter can be readily devised. In numerical simulations of two or three spatial dimensional flows such a filter can readily be applied (it will be an advantage to filter the spatial Fourier transformation of the flow). For experimental conditions where only a few probes are available for detection it is necessary to take into account that the cross section of the structure cut by the probes may not be *a priori* known, and this can require a separate statistical analysis.

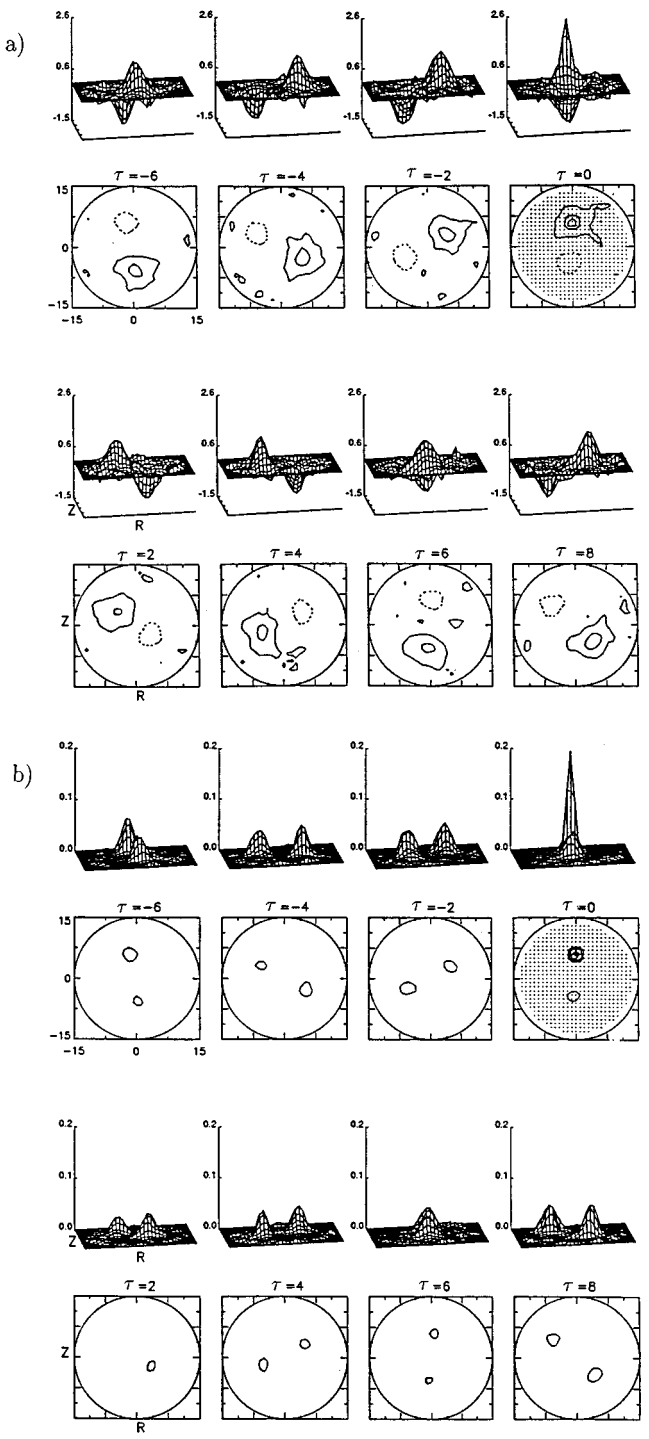

FIG. 17. Conditional analysis of the synthetic signal as a function of (R,Z) for different time steps is given in (a). The conditional reproducibility of the synthetic signal as a function of (R,Z) for different time steps is given in (b). Space and time are here measured in dimensionless computational units.

ACKNOWLEDGMENTS

We thank T. Brundtland for his expert and enthusiastic technical assistance. Without him the present work would not have been possible. Stimulating discussions with J. Trulsen and R. Armstrong are gratefully acknowledged. This work was supported in part by the Norwegian National Science Foundation.

APPENDIX

In this appendix we illustrate the performance of a conditional analysis as compared to a simple correlation between the reference signal and the one obtained from the moving probe. For this purpose, synthetic data are generated in two spatial dimensions by introducing a number of moving structures (usually two) with a prescribed form and trajectory, which propagate in a background of additive noise. The signals are recorded in a number of grid points as by the movable probe in the experimental study and analyzed by the same computer program. We carried out a number of simulations but present here only some with particular reference to the present conditions. A realistic model was obtained by having a pair of dipolelike vortices growing and decaying while rotating in the cross section. Successive structures were generated at random initial angular positions, but at a fixed radial position, and the structures were given a Gaussian amplitude time evolution. The total life cycle for a vortex was kept constant at approximately 20 time steps. The time delays between successive structures were random, but bounded so that there at a single time was no more than one dipole present, and that the maximum delay from one vortex has faded till the next appears is no longer than 50 time steps.

In Fig. 15 we show four successive snapshots beginning at an arbitrary time with structures present. The top sequence shows the signal without noise, while the bottom sequence gives the situation after adding uniformly distributed noise of amplitude ± 3.0 relative to the peak unit amplitude of one individual structure. The number of vortices passing the reference probe with an amplitude sufficiently high for detection is small in such a simulation, and it was necessary to use long time samples in order to suppress the background noise in the conditionally averaged subensembles. The correlation analysis is unsuccessful in recovering any trace of the structures in the signal, see Fig. 16. The conditional average is more successful in this respect, see Fig. 17(a). This numerical experiment also illustrated the strong dependency on the imposed condition used in the conditional sampling technique. The structures were thus *not* successfully detected when using $c=1.5$ or 2.0, in the condition $\Phi_1 > c\sigma$, but for an intermediate value of 1.8 the technique is able to reconstruct the trajectory of the vortex, and to some degree also its shape. The failure of the method when imposing a too strict condition is obvious, but the fact that a too low value for the condition c also causes structures to be missed may at first sight be surprising. The reason is that when the condition is not sufficiently high, a large number of events will be interpreted as the presence of a structure, while it in fact is the amplitude of the background noise alone that is responsible for the triggering. In this case the subensembles will be selected at arbitrary positions in the time series and the *averaged* subensembles approach the conditional average of the background noise [8]. For some cases it can therefore be expected that conditional averaging gives nontrivial results only within a *window* of imposed conditions.

To complete the analysis we obtained the conditional reproducibility as defined before, see Fig. 17(b). As the figures indicate, the conditional reproducibility may be an even better tool for determining the presence of coherent structures and their preferred trajectories than the conditional sampling method. The polarity of the structures will, however, be missed by the conditional reproducibility, which in this respect suffers from the same shortcoming as the correlation between the signals from the reference and the spatially distributed positions.

[1] H. Tasso, B. J. Green, and H. P. Zeehrfeld, Phys. Fluids **12**, 2444 (1969).
[2] K. Rypdal *et al.*, Plasma Phys. Controlled Fusion **36**, 1099 (1994).
[3] K. Rypdal, O. E. Garcia, and J.-V. Paulsen, Phys. Rev. Lett. **79**, 1857 (1997).
[4] F. Øynes, H. L. Pécseli, and K. Rypdal, Phys. Rev. Lett. **75**, 81 (1995).
[5] T. Brundtland, Vacuum **43**, 185 (1992).
[6] H. Johnsen, H. L. Pécseli, and J. Trulsen, Phys. Fluids **30**, 2239 (1987).
[7] H. L. Pécseli and J. Trulsen, Phys. Fluids B **1**, 1616 (1989).
[8] H. L. Pécseli and J. Trulsen, Phys. Scr. **43**, 503 (1991).
[9] A. V. Filippas, R. D. Bengtson, G.-X. Li, M. Meier, Ch. P. Ritz, and E. J. Powers, Phys. Plasmas **2**, 839 (1995).
[10] A. H. Nielsen, H. L. Pécseli, and J. Juul Rasmussen, Ann. Geophys. (Germany) **10**, 655 (1992).
[11] F. F. Chen, Plasma Phys. (J. Nucl. Energy, Part C) **7**, 399 (1965).
[12] D. Bora, Phys. Lett. A **139**, 308 (1989).
[13] A. H. Nielsen, H. L. Pécseli, and J. Juul Rasmussen, Europhys. Lett. **27**, 209 (1994).
[14] M. Kamitsuma, S.-L. Chen, and J.-S. Chang, J. Phys. D **10**, 1065 (1977).
[15] K. Rypdal, H. Fredriksen, J.-V. Paulsen, and O. M. Olsen, Phys. Scr. **T63**, 167 (1996).
[16] J. C. R. Hunt, N. K.-R. Kevlahan, J. C. Vassilicos, and M. Farge, in *Wavelets, Fractals and Fourier Transforms*, edited by M. Farge, J. C. R. Hunt, and J. C. Vassilicos (Clarendon, Oxford, 1993).
[17] T. Huld, A. H. Nielsen, H. L. Pécseli, and J. Juul Rasmussen, Phys. Fluids B **3**, 1609 (1991).
[18] P. Tham and A. K. Sen, Phys. Plasmas **1**, 3577 (1994).
[19] S. Benkadda *et al.*, Phys. Rev. Lett. **73**, 3403 (1994).
[20] P. Holmes, J. L. Lumley, and G. Berkooz, *Turbulence, Coherent Structures, Dynamical Systems and Symmetry* (Cambridge University Press, Cambridge, England, 1996).
[21] H. L. Pécseli, E. A. Coutsias, T. Huld, J. P. Lynov, A. H. Nielsen, and J. Juul Rasmussen, Plasma Phys. Controlled Fusion **34**, 2065 (1992).
[22] A. H. Nielsen, H. L. Pécseli, and J. Juul Rasmussen, Phys. Plasmas **3**, 1530 (1996).
[23] D. C. Champeney, *Fourier Transforms and Their Physical Applications* (Academic, London, 1973).